Advanced Materials, DOI: 10.1002/adma.201204083

SUPPORTING INFORMATION

Transient Enhancement and Spectral Narrowing of The Photothermal Effect of Plasmonic Nanoparticles Under Pulsed Excitation

By *Ekaterina Y. Lukianova-Hleb, Alexey N. Volkov, Xiangwei Wu, Dmitri O. Lapotko*

[*] Dr. Dmitri O. Lapotko
Department of Biochemistry and Cell Biology
Department of Physics and Astronomy
Rice University, 6100 Main, MS-140
Houston, TX 77005 USA
Phone: 713-348-3708
Fax: 713-348-5154
dl5@rice.edu

Dr. Ekaterina Y. Lukianova-Hleb
Departments of Biochemistry and Cell Biology
Rice University, Houston, TX 77005 USA

Dr. Alexey N. Volkov
Department of Materials Science and Engineering
University of Virginia, Charlottesville, VA 22904-4745 USA

Dr. Xiangwei Wu
Department of Head and Neck Surgery
The University of Texas
MD Anderson Cancer Center, Houston, TX 77030 USA

Methods

1. Gold nanoparticles. Solid gold spheres with diameters of 20, 60 and 120 nm were obtained from BioAssay Works LLC (Ijamsville, MD) and Ted Pella Inc. (Redding, CA). Water suspension of gold spheres was diluted to the concentrations that resulted in the inter-particle separation of > 20 μm in order to expose individual NPs to a laser beam. The suspension was sealed on a glass microscope slide with a coverslip that was separated from the bottom of the slide by a 15 μm gap by adding polystyrene spheres of this diameter (Spherotech Inc., Lake Forest, IL). After sedimentation to the bottom of the slide, the NPs were imaged with optical

scattering and were individually positioned into the center of the laser beam by using a LabView-controlled automated microscope stage (8MT167-100, Standa Ltd., Vilnius, Lithuania). Each NP was exposed only once to a single laser pulse at a specific fluence and wavelength. Signals for 40-50 NPs were obtained and statistically analyzed with the Origin 8 program (OriginLab Corporation, Northampton, MA). NP clusters (objects consisting of 10-50 aggregated particles) were prepared by adding sodium chloride to the water suspension of NPs at the concentration of NaCl 10 mg/ml and re-suspending the NP clusters in water to adjust their concentration of NP clusters to that of the single NPs. In addition, suspension samples were prepared at the increased concentration of NPs, $6.3*10^{13}$ particles/ml, in order to amplify the bulk heating effect. The suspensions were prepared in the same way as single NPs, but were used immediately after preparation, in order to minimize the effect of NP sedimentation. After each single pulse, the slide was shifted in order to avoid irradiation of the same NPs twice. An inverted microscope (Axiovert A200, Carl Zeiss MicroImaging GmbH, Germany) was used for sample manipulation. We studied three different combinations of gold spheres in water: single, clustered and suspended NPs.

2. Cells. Squamous carcinoma cells (HN31) were cultured in DMEM High Glucose medium (Cat# 10013 CV) from Mediatech supplemented with MEM Vitamin Solution (Cat# 11120) and MEM NEAA (Cat#11140), both from Gibco, and penicillin-streptomycin (Cat# 30002 CT) from Mediatech. Cells were seeded at a density of 700 000 cells per ml in the culture slides (μ Slide VI 0.4, Ibidi LLC, Martinsried, Germany). Cells were grown 24 hours in these slides before treatment with NPs. NPs were covalently conjugated with C225 antibody (Erbitux, ImClone Systems Inc., Branchburg, NJ), an antibody against the epidermal growth factor receptor that is over-expressed by HN31 cancer cells, by BioAssayWorks LLC (Ijamsville, MD). NP-C225 conjugates were incubated with the cells for 24 hours under physiological conditions and washed

from unbound NPs before PNB generation. The small size of the NPs provided efficient targeting through receptor-mediated endocytosis and the formation of intracellular NP clusters. Individual cells were positioned into the center of laser beams and were exposed to a single pulse.

3. Cell viability was measured with a Trypan Blue exclusion test. Seventy-two hours after the laser irradiation of the cells, the viabilities of intact and irradiated (single 70 ps pulse at 780 nm, 60 mJ/cm^2, the whole sample was scanned by a broad laser beam of 220 μm diameter) cells were found to be 99% and 98%, respectively. Thus, we concluded that the laser pulses did not damage the cells. All experiments were done three times.

4. Optical absorption spectra of gold NPs were obtained for suspensions of NPs and their clusters as spectra of optical density. Optical density includes both absorption and scattering components. However, for NPs with a diameter of less than 100 nm, the scattering component is negligibly small and thus optical density was used as a measure of optical absorbance. Ocean Optics Inc. spectrometer (USB 650 Red Tide spectrometer, Dunedin, FL) and software were used to compare optical absorbance at different wavelengths. The width of spectral peaks was measured at the level of 50% of the peak amplitude of the optical density or the bubble lifetime.

5. Pulsed optical excitation. We used the duration of the excitation pulse which was long enough to allow thermally-induced processes in an NP to develop (> 10 ps), and short enough to prevent significant development of the secondary environmental phenomena due to heat transfer. These phenomena are heat dissipation (100-1000 ps), evaporation and bubble expansion (>100 ps) and total destruction of the NP. Use of a single pulse avoided the influence of any irreversible changes in the NP during its interaction with excitation radiation. Therefore, we employed 70 ps pulses with high pulse-to-pulse energy stability and Gaussian intensity profile at wavelengths close to the plasmon resonance of gold spheres (532 nm) and tunable in the NIR region from 720 to 900 nm (PL-2250, Ekspla, Vilnius, Lithuania). The width of laser line was about 0.4 nm in

NIR (780 nm). The laser beam was directed into a sample through a focusing lens with the beam diameter at the sample plane being 14 μm (Figure S1). We used a tunable pulsed micro-laser STH-01SH (Standa Ltd, Vilnius, Lithuania) as the source of the visible and NIR pulses with a duration of 400 ps. The laser fluence was controlled with an attenuator and was measured by a calibrated energy meter (Ophir Optronics, Ltd., Israel) and by imaging the laser spot in the object plane with an image detector (EM CCD camera, Luka model, Andor Technology, Northern Ireland). The diameter of the Gaussian laser beam was measured at the level $1/e^2$ relative to its maximal image pixel amplitude in the center of the beam.

6. Measurement of the pulsed photothermal output of NPs. The laser pulse-induced temperatures assume the formation of a transient thermal field and vapor nanobubble around an NP. Thermal output below the bubble threshold was quantified through the bulk heating of water and measured with a thermal lens method[1] as an amplitude of the thermal lens trace (time-response). This trace was detected with a continuous stabilized 633 nm laser (<0.1 mW, 05-STP-901, CVI Meller Griot, Albuquerque, NM) that was focused onto a sample collinearly to the excitation laser beam (Figure S1). The axial intensity of the probe beam was monitored in a far field after the sample with a photodetector (FPD510-FV, Thorlabs Inc., Newton, NJ), whose output was analyzed by a digital oscilloscope (Lecroy X42 WaveSurfer, LeCroy Corporation) as the thermal trace. A vapor nanobubble was detected with the same probe laser with the trace having a bubble-specific shape due to its scattering effect during expansion and collapse. We used the nanobubble lifetime, τ_{PNB}, as a photothermal metric.[2] The lifetime was measured as the duration (not the amplitude) of the nanobubble trace at the level of half of the maximal amplitude of the signal. This metric describes the thermal energy generated by the NP: nanobubble lifetime is proportional to its maximal diameter that, in turn, determines the bubble energy.[3] Since the vapor around an NP almost blocks any thermal diffusion from the NP to the water outside the

bubble[2], we can consider that, for fluence levels well above the nanobubble generation threshold, all thermal energy released by the NP is equal to the bubble energy, and thus can be expressed through the directly measurable lifetime. This energy is a part of the absorbed energy that is split between the released energy and the energy utilized for NP heating and modification. Considering the latter as a constant, we can directly correlate the nanobubble lifetime to an efficient absorption cross-section of the NP, the parameter that determines the photothermal efficacy of the optical absorber:

$$E_{abs} = E_0 * \sigma_{abs} = \tau_{PNB} * K + const \quad (1)$$

where coefficient *K* connects τ_{PNB}, and the bubble energy[3].

In stationary case σ_{abs} does not change during absorption of the laser pulse and is easily measured through the optical density of the NP suspension as an extinction spectrum. This is because, for small enough NPs (<100 nm), the extinction coefficient almost coincides with the absorption coefficient. During the dynamic modification of the NP and the potential formation of the additional transient structures with their own optical absorption, we can consider sigma as an integral parameter that is not formally a constant but is a complex function of the NP and transient structure. Nevertheless, it can still be used to describe the integral optical absorbance for the specific duration, fluence and wavelength of the excitation laser pulse.

Using the model described above, we measured the photothermal (PT) properties of gold spheres as the function of the excitation wavelength for several parameters and conditions: single NP, cluster of aggregated NPs and individual live cells with internalized NPs. The PT properties of the NP at stationary ambient conditions were obtained though the spectrum of optical density of the NP suspension. The amplification factor was calculated for 780 nm by normalizing the ratio of the nanobubble lifetimes at 780 nm (τ_{PNB}^{780}) and 532 nm (τ_{PNB}^{532}) (obtained under identical

optical fluence) by the ratio of absorption cross-sections (that usually describe the photothermal efficacy at ambient stationary conditions[4,5]) at the same wavelengths:

$$K_{amp} = (\tau_{PNB}^{780}/\tau_{PNB}^{532})/(\sigma_{abs}^{780}/\sigma_{abs}^{532}) \quad (2),$$

Absorption cross-sections of gold spheres were calculated for ambient temperatures using Mie theory[6,7] and the model and algorithm developed earlier[8].

The acoustic detection of nanobubbles in opaque tissue employed an XMS-310 ultrasound transducer (Olympus NDT Inc., Waltham, MA) coupled to a pre-amplifier (Ultrasonic *Preamp 5676,* Olympus NDT Inc., Waltham, MA). The output of the amplifier was registered as the acoustic trace of the nanobubble with the oscilloscope. To correlate the acoustic and optical methods of nanobubble detection, we measured the amplitude of the acoustic trace as a function of the nanobubble lifetime measured optically. The experiment was performed for individual cells and the acoustic and optical traces were simultaneously detected during exposure of each individual cell to a single laser pulse. We observed an almost linear correlation between these two parameters, which justified using acoustic amplitudes instead of the nanobubble lifetimes in opaque tissues (these procedure and data are described in detail in Ref. 9). In the animal experiment, the ultrasound transducer was pressed to a tissue through an ultrasound gel (Aquasonic 100, Parker Laboratories, Inc., Fairfield, NJ) at the distance of 2-3 mm from the irradiated area. In order to verify the origin of acoustic traces, they were obtained for a wide range of laser fluences for the tumor and normal tissue (Figure 2D), at the NIR wavelength of 780 nm and at the wavelength close to the plasmon resonance of gold spheres, 532 nm. We observed a steady increase of the acoustic amplitude only in the tumor (that preferably accumulated gold NPs through the mechanism of the receptor-mediated endocytosis [10, 11]), but not in normal tissue (see also p.8 below). The small acoustic signal observed in normal tissues (Figure 1E) can be attributed to the contribution of residual, non-specifically accumulated or not

fully cleared gold NPs that did not generate nanobubbles, but provided some background signal due to the regular photoacoustic effect of single NPs.[12]

7. The electron microscopy evaluation of gold NPs was performed in transmission electron microscopy (TEM) mode of a Hitachi H-7500 (Hitachi High Technology America, Inc., Schaumburg, IL) microscope at 100000 magnification. Two metrics were determined for intact and laser-treated gold NPs. Average NP diameter D (nm) was measured for 80-100 individual NPs. Surface roughness $R\ (\%) = (D_{max} - D_{min})/D\ x100$ was measured for each of 80-100 NPs as the relative difference between the maximal (D_{max}) and minimal (D_{min}) diameters found for each NP. The NP samples for TEM were prepared by scanning the whole area of the well (thus exposing 100% of NPs in the suspension) laser beam at specific wavelength and fluence. Laser beam diameter, scan speed and the laser repetition rate were synchronized to provide single pulse treatment conditions for all NPs.

8. Modeling of the initial thermal response of the NP to a single short laser pulse. The one-dimensional hydrodynamic model[13] was applied in order to calculate the temperature of a gold NP in water heated by a single laser pulse with a Gaussian temporal profile. The simulations were aimed at the estimation of the time that is required to heat the NP surface up to temperatures that support the surface melting of the NP. The influence of the vapor nanobubble formation, NP heating and melting on the optical absorbance of the NP was analyzed by us in detail previously[8], as well as the optical scattering effects of the expanding vapor nanobubble.[2] This model considered only the initial heating stage before the vapor nanobubble develops (vapor changes the optical constants of gold, scatters the incident excitation laser pulse and influences heat transfer). We also did not consider NP melting (this also changes its optical absorbance), thermal disintegration or the corresponding dynamic change in the optical absorption cross-section of the NP, as their influence was previously analyzed by us in detail.[2]

Preliminary simulations showed that, under the conditions considered in Figure 1A, the initial temperature and pressure in the water-gold NP system are equal to 293 K and 10^5 Pa, respectively, an absorption cross-section of 60 nm gold NP σ_a is chosen to be equal to 10^{-12} cm^2 that corresponds to 780 nm laser wavelength. The maximum laser pulse intensity occurs at 0.119 ns. The effects of electron-lattice non-equilibrium in the NP material and thermal expansion of the NP are relatively small and can be neglected. The homogeneous NP temperature, $T_p(t)$, is then determined by the equation accounting for the laser heating of the NP and its cooling by the surrounding water:

$$m_p C_p \frac{dT_p}{dt} = \sigma_a I_L(t) - \pi d_p^2 q_w, \tag{3}$$

where t is the time, $V_p = (1/6)\pi d_p^3$ and $m_p = \rho_p V_p$ are the volume and mass of a particle with diameter d_p and density ρ, q_w is the heat flux at the NP surface, C_p is the specific heat of the NP material, σ_a is the NP absorption cross section, $I_L(t) = F_L \exp\left(-(t-3t_\sigma)^2/2t_\sigma^2\right)/\sqrt{2\pi}t_\sigma$ is the intensity of the incident laser irradiation, $t_\sigma = t_L/2\sqrt{2\ln 2}$, F_L and t_L are the incident laser fluence and the laser pulse duration, respectively (full width at half maximum of the Gaussian laser pulse). For a gold NP, simulations are performed with ρ_p=*19300 kg/m*^{3} and C_p=*143.6 J/kg*K*.[13]

One-dimensional, spherically symmetric mechanical and thermal processes, evolving in water due to heating at the water/NP interface, are described by the Navier-Stokes equations[14]

$$\frac{\partial \rho}{\partial t} + \frac{\partial(\rho v_r)}{\partial r} + \frac{2}{r}\rho v_r = 0, \tag{4}$$

$$\rho\left(\frac{\partial v_r}{\partial t} + v_r \frac{\partial v_r}{\partial r}\right) = -\frac{\partial p}{\partial r} + \frac{\partial \tau_{rr}}{\partial r} + \frac{3}{r}\tau_{rr}, \tag{5}$$

$$\rho\left(\frac{\partial \varepsilon}{\partial t}+v_r\frac{\partial \varepsilon}{\partial r}\right)=-\frac{\partial q_r}{\partial r}-\left(p-\tau_{rr}\right)\frac{\partial v_r}{\partial r}-\frac{2}{r}\left[\left(p-\tau_{rr}+\frac{3}{2}\tau_{rr}\right)v_r+q_r\right], \tag{6}$$

where r is the distance from the center of the NP, ρ, v_r, ε and p are the density, velocity in r-direction, specific internal energy, and the pressure of the fluid; τ_{rr} is a diagonal component of Newton's viscous stress tensor; q_r is the component of the heat flux vector in r-direction which is described by Fourier's law:

$$\tau_{rr}=\frac{4}{3}\mu\left(\frac{\partial v_r}{\partial r}-\frac{v_r}{r}\right), \qquad q_r=-\kappa\frac{\partial T}{\partial r}, \tag{7}$$

where μ, κ, and T are the viscosity, thermal conductivity, and temperature of the water, respectively.

The thermal, $p=p(\rho,T)$, and caloric, $\varepsilon=\varepsilon(\rho,T)$, equations of state for liquid water in Eqs. (4)-(6) are calculated based on the equation of state recommended for general and scientific use by the International Association for the Properties of Water and Steam (IAPWS) in IAPWS95.[15] Since the purpose of these simulations is to estimate only the initial stage of NP heating, all simulations were performed with the one-phase equation of state for liquid water, neglecting the formation of a vapor layer insulating the NP from the liquid. It is worth noting that recent molecular dynamics simulations also showed that the surface tension pressure around a 60 nm sphere can inhibit the boiling of water and thus can support further heating of the NPs up to the bulk melting temperature (1337 K) without the active expansion of a vapor bubble.[16,17] The temperature-dependent thermal conductivity and viscosity of liquid water are calculated based on tabulated data from recent IAPWS releases.[18,19]

Eqs. (3)-(7) are solved with the boundary and initial conditions as follows

$$\text{at } r=R_p=d_p/2:\ v_r(R_p,t)=0,\ T(R_p,t)=T_p(t),\ q_w(t)=q_r(R_p,t), \tag{8}$$

$$\text{at } r = R_e: \; v_r(R_e,t) = 0, \; T(R_e,t) = T^0, \tag{9}$$

$$\text{at } t = 0: \; \rho(r,0) = \rho^0, \; v_r(r,0) = 0, \; T(r,0) = T^0, \quad T_p(0) = T^0, \tag{10}$$

where ρ^0 is the liquid density which corresponds to the initial temperature T^0 and pressure p^0, and R_e is the distance from the particle center to the external boundary of the computational domain. In simulations, R_e is chosen to be large enough, so that the pressure and thermal waves induced by the NP heating do not reach the external boundary during the simulated time.

The problem posed by Eqs. (3)-(10) was solved numerically by using the scheme of the second order of approximation in time and space based on the splitting method. In particular, the convective part of Eqs. (4)-(6) was solved by the Richtmayer scheme[20] and the diffusion part was solved by the central difference scheme[20].

The conditions at the NP surface given by Eq. (8) do not account for the effect of thermal boundary resistance at the NP-water interface, which is known to be important based on results of atomic-level simulations.[16,17] These conditions, however, are quite satisfactory for the current task. An additional thermal resistance of the NP-water interface will delay the heat flow from the NP into water, thus increasing the initial temperature of the NP and shortening the time intervals between the beginning of the laser pulse and the onset of the NP surface melting. We did not analyze the temperature after onset of the water vapor phase around the NP.

9. Animals. Healthy, male athymic nude mice, age 8 to 12 weeks, were used in our experiments and they were purchased from the animal production area of the National Cancer Institute-Frederick Cancer Research and Development Center (Frederick, MD). An orthotopic xenograft model, in which the tumor cells are implanted in the tumor site of origin, was used. The tumors were induced with human head and neck squamous carcinoma HN31 cells on the mice flanks: the nude mice were anesthetized and $1x10^6$ HN31 cells were injected using a 1-ml tuberculin syringe

with a 30-gauge hypodermic needle. 14 to 17 days after the injection of cells, when tumors are already established (5-6 mm in diameter), the C225-conjugated 60nm gold spheres diluted by serum-free Dulbecco's modified Eagle's medium were intravenously slowly injected (0.8μg/g body weight) into the tail vein using an intravenous catheter and a 1-ml-insulin-syringe. Twenty-four hours after the injection of the NPs, the mice were anesthetized, skin was removed in an area of laser treatment (tumor and adjacent tissue) and nanobubbles were generated and detected. The acoustic amplitudes of the nanobubbles were obtained for the tumor and normal tissue as the spectrum during the *in vivo* excitation of gold NPs with single laser pulses at 40 mJ/cm^2.

The mice were housed and maintained in laminar flow cabinets under specific pathogen-free conditions in the facilities of the M. D. Anderson Cancer Center. These facilities were approved by the American Association for Accreditation of Laboratory Animal Care in accordance with current regulations and standards of the U.S. Department of Agriculture, the U. S. Department of Health and Human Services, and the National Institutes of Health. The mice were used in accordance with the Animal Care and Use Guidelines of M. D. Anderson Cancer Center under a protocol approved by the Institutional Animal Care Use Committee. All procedures causing discomfort were performed under anesthesia (an intraperitoneal injection of a 1.2% avertin solution, 0.2ml/10g body weight). Mice were observed daily for their level of activity and normal eating, drinking and grooming behavior. If a mouse demonstrated marked weight loss, had ruffled fur and showed difficulty walking, it was removed from the study and euthanatized with carbon dioxide gas. This method of euthanasia is consistent with the guidelines set by the panel on Euthanasia of the American Veterinary Medical Association.

10. Tissue viability was analyzed 72 hours after laser irradiation. The fully irradiated and intact tumors were extracted 72 hours after laser irradiation, fixed with 10% formalin for 48 hours, embedded in paraffin and prepared by the standard technique for hematoxylin-eosin (H&E)

staining. For the analysis of tissue necrosis, the tumors were sliced in the direction of propagation of laser radiation. The level of the necrosis in the intact and laser-treated tumors was measured for the surface and sub-cutaneous tissues from the depth of 0 to 2 mm. The intact tumor yielded a 2±3 % level of necrosis and the laser-treated tumor yielded a 6±4% level of necrosis. Therefore, a single pulse laser treatment did not cause any detectable toxic effect in irradiated tissues.

References

(1) Tam, A. C. *Rev Mod Phys* **1986**, *58*, 381-431.

(2) Lukianova-Hleb, E., Hu, Y., Latterini, L., Tarpani, L., Lee, S., Drezek, R.A., Hafner, J.H., Lapotko, D.O. *ACS Nano* **2010**, *4*, 2109-2123.

(3) Plesset, M. S. *Trans ASME: J Appl Mechanics* **1949**, *16*, 277-282.

(4) Kreibig, U., Vollmer, M. *Optical properties of metal clusters* (Springer-Verlag, Berlin, Heidelberg, 1995).

(5) Hartland, G. V. *Annu Rev Phys Chem* **2006**, *57*, 403-430.

(6) Mie, G. *Ann Phys Leipzig* **1908**, *25*, 377–445.

(7) Bohren, C. F.; Huffman, D. R. *Absorption and scattering of light by small particles* (Wiley Interscience, New York, 1983).

(8) Lukianova-Hleb, E.Y., Sassaroli, E., Jones, A., Lapotko, D. O. *Langmuir* **2012**, *28*, 4858-4866.

(9) Lukianova-Hleb, E. Y.; Belyanin, A.; Kashinath, S.; Wu, X.; Lapotko, D. *Biomaterials* **2012**, *33*, 1821-1826.

(10) Lukianova-Hleb, E. Y.; Ren, X.; Zasadzinski, J. A.; Wu, X.; Lapotko, D. *Adv Mater* **2012**, DOI: 10.1002/adma.201103550.

(11) Lapotko, D.; Lukianova-Hleb, E.; Oraevsky, A. *Nanomedicine* **2007**, *2*, 241–253.

(12) Xu, X.; Liu, H.; Wang, L.V. *Nature Photonics* **2011**, *5*, 154-157.

(13) Volkov, A. N., Sevilla, C., Zhigilei, L. V. *Appl. Surf. Sci.* **2007**, *253*, 6394-6399

(14) Sedov, L. I. Mechanics of Continuous Media, Vol. 1 (World Scientific, Singapore, 1996).

(15) Wagner, W., Pruß, A., *J. Phys. Chem. Ref. Data* **2002***, 31*, 387.

(16) Merabia, S., Keblinski, P., Joly, L., Lewis, L. J., Barrat, J. L. *Phys. Rev. E* **2009**, *79*, 021404.

(17) Merabia, S., Shenogin, S., Joly, L., Keblinski, P. Barrat, J. L. *Proc. Natl. Acad. Sci. U.S.A.* **2009**, *106*, 15113-15118.

(18) Revised Release on the IAPS Formulation 1985 for the Thermal Conductivity of Ordinary Water Substance (International Association for the Properties of Water and Stream, 1998) http://www.iapws.org/

(19) Revised Release on the IAPS Formulation 1985 for the Viscosity of Ordinary Water Substance (International Association for the Properties of Water and Stream, 2003) http://www.iapws.org/

(20) Toro, E. F. *Riemann Solvers and Numerical Methods for Fluid Dynamics* (Springer, Berlin, 1999).

Supporting figures

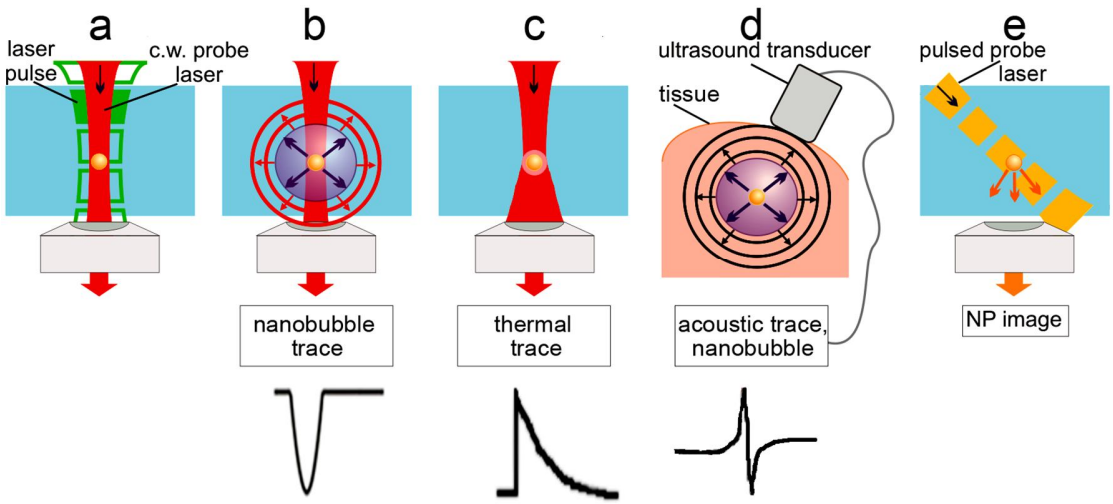

Figure S1. The experimental generation and detection of the transient photothermal effects in gold nanospheres (NPs) with a photothermal microscope (A-C, E). (A) The NP is exposed to a focused collinear single excitation laser pulse with tunable wavelength and fluence, and to a continuous probe laser beam (633 nm). (B) The optical scattering effect of the expanding and collapsing vapor nanobubble reduces the axial intensity of the continuous probe laser beam and thus delivers the nanobubble-specific time-response (trace) of the photodetector. (C) The bulk heating of the water around the NP creates a thermal lens effect on the continuous probe laser beam and thus delivers a time-response (trace) specific to the heating-cooling cycle. (D) The acoustic detection of a nanobubble in opaque tissue with an ultrasound transducer. (E) Optical scattering imaging of NP with a pulsed probe laser is used for positioning the individual NP in the center of the excitation pulsed laser beam.

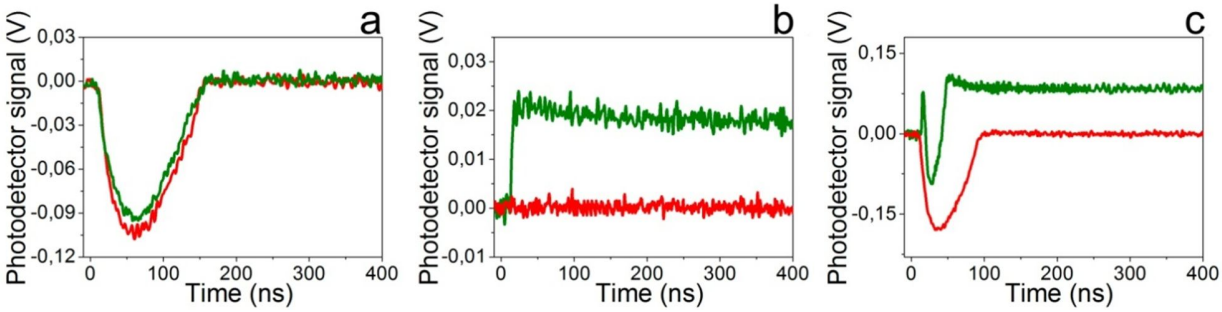

Figure S2. Optical traces (time-responses) of individual 60 nm gold spheres exposed to a single 70 ps laser pulse at 532 nm (*green*) and 780 nm (*red*) at various fluence levels: (A) above the nanobubble generation threshold (responses show a bubble-specific shape that corresponds to the expansion and collapse of the vapor nanobubble); (B) below the nanobubble generation threshold (sharp front and long tail characterize, respectively, bulk water heating and cooling by gold spheres); (C) near the nanobubble generation threshold for 532 nm (at 532 nm some spheres generate nanobubbles while some still heat the water, while at 780 nm much larger nanobubbles are generated without any bulk heating effect).

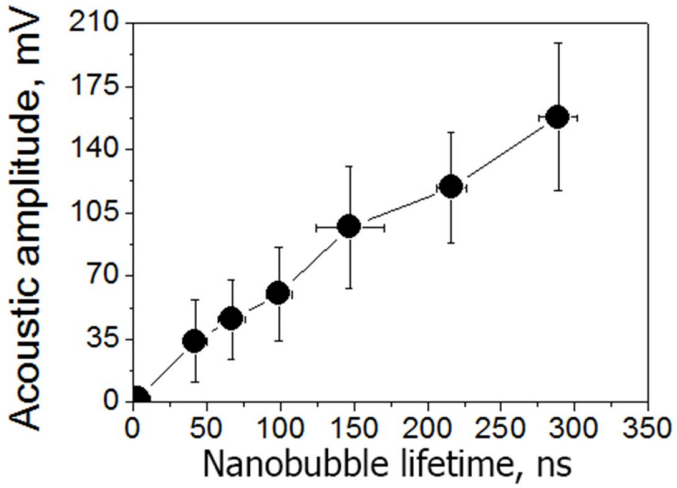

Figure S3. Dependence of the acoustic amplitude upon optically measured lifetime of nanobubbles.

Supporting Tables

Table S1. Near-infrared performance of gold NPs under single pulse excitation

Sample	**Stationary excitation**			**No-stationary excitation**			**Spectral narrow-wing** (ratio of peak width non-stationary/ stationary)	**Photo-thermal ampli-fication,** ($K_{amp} = (\tau^p_{PNB}/\tau^m_{PNB}) / (\sigma^p_{abs}/\sigma^m_{abs})$)
	Peak wave-length, nm	Peak width, nm	Ratio of optical absorption cross-sections at non-stationary/ stationary peaks	Peak wave-lengt, nm	Peak width, nm	Ratio of nano-bubble lifetimes at non-stationary/ stationary peaks $\tau^p_{PNB}/\tau^m_{PNB}$		
Single 60 nm gold spheres in water								
Laser pulse fluence 230 mJ cm^{-2}	555	110	0.009	780	1.5	1.13	97	125
Laser pulse fluence 66 mJ cm^{-2}	555	110	0.009	780	4.5	0.79	24	88
Single clusters of gold spheres in water								
20 nm	532	162	0.007	780	3.5	0.7	46	95
60 nm	555	198	0.009	780	10	0.82	20	91
Suspension of gold spheres in water								
20 nm	532	90	0.007	780	8	0.5	11	68
60 nm	555	110	0.009	780	11	0.65	10	72
120 nm	580	220	0.058	780	4	0.87	55	15
C225 conjugates of gold spheres clustered in HN31 cells *in vitro*								
20 nm	532	162	0.007	780	2.2	0.98	74	132
60 nm	555	198	0.009	780	2.5	0.65	79	72
C225 conjugates of gold spheres clustered in tumor *in vivo*								
60 nm	555	198	0.009	780	3	0.86	66	95